Structural insights into the main S-layer unit of *Deinococcus radiodurans* reveal a massive protein complex with porin-like features

Received for publication, December 8, 2019, and in revised form, February 13, 2020 Published, Papers in Press, February 18, 2020, DOI 10.1074/jbc.RA119.012174

Domenica Farci[‡1], Mehmet Alphan Aksoyoglu[§], Stefano Francesco Farci[¶], Jayesh Arun Bafna[§], Igor Bodrenko[‖], Matteo Ceccarelli[‖], Joanna Kirkpatrick[‡‡], Mathias Winterhalter[§], Sami Kereïche[§§2], and Dario Piano[‡3]**

From the [‡]Department of Plant Physiology, Warsaw University of Life Sciences–SGGW, Nowoursynowska Str. 159, 02776 Warsaw, Poland, the [§]Department of Life Sciences and Chemistry, Jacobs University Bremen, 28759 Bremen, Germany, the [¶]Laboratory of Plant Physiology and Photobiology, Department of Life and Environmental Sciences, University of Cagliari, V.le S. Ignazio da Laconi 13, 09123 Cagliari, Italy, the [‖]Department of Physics and IOM/CNR, University of Cagliari, 09042 Monserrato, Italy, the [**]Leibniz Institute on Ageing–Fritz Lipmann Institute, Beutenbergstrasse 11, 07745 Jena, Germany, [‡‡]The Francis Crick Institute, 1 Midland Road, NW1 1AT London, United Kingdom, and the [§§]Institute of Biology and Medical Genetics, First Faculty of Medicine, Charles University, Prague 128 00, Czech Republic

Edited by Mike Shipston

In the extremophile bacterium *Deinococcus radiodurans*, the outermost surface layer is tightly connected with the rest of the cell wall. This integrated organization provides a compact structure that shields the bacterium against environmental stresses. The fundamental unit of this surface layer (S-layer) is the S-layer deinoxanthin-binding complex (SDBC), which binds the carotenoid deinoxanthin and provides both, thermostability and UV radiation resistance. However, the structural organization of the SDBC awaits elucidation. Here, we report the isolation of the SDBC with a gentle procedure consisting of lysozyme treatment and solubilization with the nonionic detergent *n*-dodecyl-β-D-maltoside, which preserved both hydrophilic and hydrophobic components of the SDBC and allows the retention of several minor subunits. As observed by low-resolution single-particle analysis, we show that the complex possesses a porin-like structural organization, but is larger than other known porins. We also noted that the main SDBC component, the protein DR_2577, shares regions of similarity with known porins. Moreover, results from electrophysiological assays with membrane-reconstituted SDBC disclosed that it is a nonselective channel that has some peculiar gating properties, but also exhibits behavior typically observed in pore-forming proteins, such as porins and ionic transporters. The functional properties of this system and its porin-like organization provide information critical for understanding ion permeability through the outer cell surface of S-layer–carrying bacterial species.

In several groups of Bacteria and Archaea, the first line of defense against environmental shocks consists of a protective shield called the surface layer (S-layer).[4] This structure is anchored and intimately connected to the underlying outer membrane (1–7). S-layers appear as proteinaceous paracrystalline surfaces, and they are often associated with resistance to extreme environmental conditions (8–12). Representing the interface between cells and environments, S-layers are involved in a wide variety of essential functions, including the cell adhesion, the resistance to extreme conditions, and the maintenance of cell shape and rigidity (4, 13–15). Therefore, to understand how S-layers carrying bacteria interact with their environment, it is essential to determine the arrangement and role of their main outermost proteinaceous constituents. The properties of S-layer proteins, such as stability, self-assembly, and isoporosity (4), not only make them an interesting subject for studying the defensive strategies used by bacteria, but also useful targets with potential for nano- and biotechnological applications (16, 17). Despite their importance, there is a distinct lack of high-resolution structural data available for these proteins. S-layers were first observed in 1975 by EM (1), and subsequently, a large amount of genetic and biochemical data has been generated on S-layers from bacteria and archaea (1–10). The self-assembling properties of these proteins naturally lend themselves to the technique of electron crystallography, and many pioneering studies have produced projection maps and 3D reconstructions from reconstituted S-layer proteins (18). More recently, high-resolution structural data have become available, in particular

This work was supported by National Science Center (Poland) Sonata BIS 7 Program (2017) Grant PRO-2017/26/E/NZ1/00344 (to D. P. and D. F.), L'Oréal-UNESCO Fellowship for Women in Science 2017, Italy (L'Oréal Italia Per le Donne e la Scienza) (to D. F.), Czech Science Foundation Grant 1825144Y (to S. K.), the core facility Cryo-Electron Microscopy and Tomography, CEITEC, Brno, Czech Republic, and National Science Center (Poland) Harmonia 10 Program (2018) Grant PRO-2018/30/M/NZ1/00284 (to D. P. and D. F.). The authors declare that they have no conflicts of interest with the contents of this article.

This article contains Figs. S1–S3 and Table S1.

[1] To whom correspondence may be addressed. E-mail: domenica_farci@sggw.pl.

[2] To whom correspondence may be addressed. E-mail: sami.kereiche@lfl.cuni.cz.

[3] To whom correspondence may be addressed. Tel.: 48604651197; E-mail: dario_piano@sggw.pl or dario.piano@yahoo.it.

[4] The abbreviations used are: S-layer, surface layer; SDBC, S-layer deinoxanthin-binding complex; β-DDM, *n*-dodecyl-β-D-maltoside; SEC, size-exclusion chromatography; nS, nanosiemens; SLH, S-layer homology; Omp, outer membrane protein; Opr, outer membrane porin; DPhPC, 1,2-diphytanoyl-*sn*-glycero-phosphatidylcholine; BN, Blue Native.

by resolving the crystal structure of the main S-layer proteins from *Geobacillus stearothermophilus* (19) and *Caulobacter crescentus* (20).

In *Deinococcus,* a complex-layered cell envelope supports a proteinaceous S-layer (21). Among the *Deinococcus* species, *Deinococcus radiodurans* has been extensively studied for its extreme radioresistant features and its S-layer (22–27). These studies resulted in a wealth of biochemical data and structural information obtained by different techniques such as EM, electron crystallography, and atomic force microscopy (21, 28–31). These data provided a detailed overview of the S-layer structural arrangement identifying a characteristic organization and a system of regular pores, which has been shown to switch from an open to a closed state (32). On its surface, this S-layer appears as a hexagonal paracrystalline plane that covers the outer membrane (28, 32, 33), but molecular details of its attachment to and assembly within the underlying cell envelope remain unknown. The S-layer of *D. radiodurans* was thought to be mostly composed of a single polypeptide, the protein DR_2508, that forms closely-packed particles on the outer surface. Because of the symmetry of this complex, these unitary particles are called hexagonally-packed intermediates (28, 34). On the contrary, it has been recently shown that several protein complexes are actually involved in the organization of this S-layer (33). In particular, the protein DR_2577, also known as SlpA, has been identified as a main S-layer protein pivotally contributing to the integrity of the cell envelope (33, 35, 36). On the basis of these new observations, the model for this S-layer was reviewed showing not only the main biochemical, structural, and functional role played by the protein DR_2577 (11, 12, 33, 36, 37) but also that one of the multiprotein complexes composing this S-layer could span both the inner and the outer membrane (33). These observations comply with a model where the S-layer of *D. radiodurans* is one part of a much more complex structure, which is believed to be a sequence of layers stacked upon the external surface of the outer membrane (28, 35). Therefore, the revised model implies an integrated organization of the cell wall layers, in which the regularity of the S-layer could be extended to the layers below (33). Recently, it was also shown that the protein DR_2577 is not only the main S-layer component, but also that it functionalizes this structure by binding the carotenoid deinoxanthin (11, 12). This protein complex, called S-layer deinoxanthin binding complex (SDBC), behaves as a shield against UV radiation and stabilizes the S-layer and the bacterium against thermal stress (11, 12). In this study, starting from homogeneous cell wall fragments, we have isolated the SDBC with a new procedure characterized by conditions more gentle than previously reported. This procedure preserves both the hydrophilic and hydrophobic component of the SDBC allowing the retention of several minor subunits. Here, we demonstrate the following. (i) The SDBC is organized in a porin-like structure, but has larger dimensions if compared with other known porins. (ii) The main component of the complex, the protein DR_2577, shares regions of similarity with known porins. (iii) The complex shows a behavior typically observed in pore-forming proteins, such as porins and ionic transporters, when subjected to electrophysiology assays. (iv) The SDBC has minor subunits that might be auxiliary to the transport of small molecules and ions across the cell wall. Among these points, considering that the primary sequence of S-layer proteins is typically poorly conserved, except for the S-layer homology domain (SLH) (38), the significant similarity between porins and regions of DR_2577 is of primary relevance. Accordingly, this similarity and the related structural and functional features identified for the SDBC are presented here taking into account that the S-layer proteins are the evolutive result of recombination events (38–40), thus bringing a great structural and functional species-specific variability. The data shown here provide the first insights on the relationship between structure and function of the SDBC, adding important elements in our understanding of this S-layer and its interaction with the rest of the cell wall.

Results

SDBC isolated under mild conditions retains several minor subunits

After lysozyme treatment, to isolate and identify the main S-layer complexes, we have subjected the cell wall fragments to a mild solubilization with the nonionic detergent β-DDM, which was also kept in all the buffers subsequently used. Before solubilization, the quality of the cell wall fragments was evaluated by transmission EM (Fig. 1), and after solubilization, the quality was evaluated by SDS-PAGE (Fig. 2). The soluble fraction was subjected to a first step of ion-exchange chromatography, through which a main peak composed of several fractions could be isolated (elution peak P, Fig. S1*a*). The quality of the fractions was confirmed by the characteristic pink color of the SDBC and a reproducible pattern of bands on SDS-PAGE (Fig. S1*a*). The fractions were then pooled, concentrated, and subjected to a step of size-exclusion chromatography (SEC), which eventually allowed us to obtain pure SDBC samples carrying a high molecular weight and retaining the carotenoid deinoxanthin (Fig. S1*b*). Both these properties are in line with previous reports that have described the SDBC as a hexameric complex of the protein DR_2577 (36) with the carotenoid deinoxanthin bound to it (41). This mild procedure also allowed the isolation of the SDBC complex bound to its minor subunits, as observed by a characteristic and reproducible pattern of bands associated with the dominant and heavier DR_2577 band in SDS-PAGE (Fig. 2). Contrary to this procedure, the previously reported one (36) allows the only isolation of DR_2577 hexamers, the homo-oligomeric component of the SDBC. The rationale of these differences will be discussed below.

Main S-layer complex of D. radiodurans has a porin-like shape but carries a higher mass with respect to porins

To further characterize this hetero-oligomeric form of the SDBC, the pool of fractions collected by SEC was subsequently analyzed by negative stain EM. Images of this sample revealed a homogeneous field of the same particle, which appeared to be a large complex exhibiting a strong 3-fold symmetry (Fig. 3*a*). From the 2D average, top views of particles appeared with a triangular shape, having a 20-nm side, and with the surface organized into three pores according to what seems to be a 3-fold symmetry (no symmetry was imposed during processing, see Fig. 3*b* and Fig. S2), as also observable on tilted top views

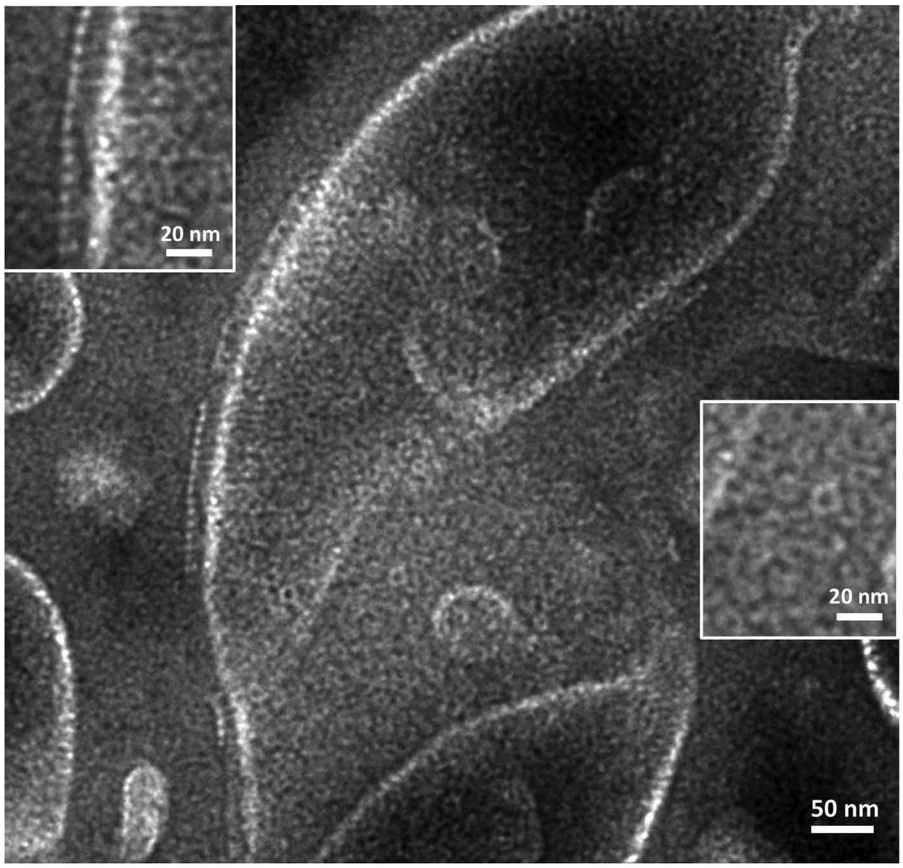

Figure 1. Electron micrograph of isolated cell wall fragments. Negatively-stained samples show the integrity of the cell wall fragments and their typical regular repetition of units; *insets* are positioned to show side-view detail (*top left*) and top-view detail (*bottom right*) of the structural units' repetition. *Scale bars* are indicated.

(Fig. 3*c* and Fig. S2). Side views and tilted side views of this complex showed a typical needle structure departing from the center of the triangle corresponding to its 3-fold symmetry axis (Fig. 3, *c–e,* and Fig. S2). In this respect, side views have a thickness of ~3.5 nm and can be classified into two categories: particles with extra arch-shaped densities stabilizing the needle-like domain and keeping it straight (Fig. 3*e* and Fig. S2), and particles where the absence of these extra densities led to the random bending of the needle-like domain (Fig. 3*d* and Fig. S2). Bottom views were difficult to obtain in large numbers (Fig. 3*f*), possibly due to the needle-like structure present on the top side of the complex, which might induce a preferential orientation. The mass of this complex was estimated by several approaches (Table 1) showing it in all cases to be >800 kDa. The overall structure of this complex strongly resembles a porin, but is several times bigger (42).

SDBC shares a region of local homology with porins

To understand whether the structural porin-like features were also related to the presence of functional domains, the similarity between porins and the DR_2577, the main SDBC component in mass and subunits (Fig. 2), was estimated. In particular, the DR_2577 sequence was compared with the porin Omp38 (Uniprot ID, Q6RYW5) from *Acinetobacter baumannii* and the porin O (OprO, Uniprot ID, P32977) from *Pseudomonas aeruginosa*, both organisms that carry an S-layer (43–45). The alignment with the Omp38 showed a local similarity of ~28% from residues 376 to 763, whereas a blind analysis with the HHpred software (see below details) gave, for the same DR_2577 region, a local similarity of ~21% with the Porin O (46). Among these two proteins, only Porin O has a tertiary structure (Protein Data Bank code 4rjw) comparable with the DR_2577 predicted structure (Fig. 4) (37). This result supported a possible porin-like function suggesting further investigations.

SDBC retains subunits that may be essential for gating substrates in/out of the cell

Concentrated SDBC samples showed a typical pattern of bands, suggesting the SDBC to interact with other minor subunits, thereby supporting the hypothesis of being a hetero-oligomeric complex *in vivo*. To clarify this, the whole subunits, including the less represented ones, were identified through mass spectrometry analyses. A summary of the protein entries identified for each SDBC component resolved by SDS-PAGE (Fig. 2) is reported in Tables 2 and Table S1. Apart from the presence of DR_2577 strongly associated with band 1 (B1), we observed several other unknown proteins associated with the other bands. In detail, band 2 (B2) was identified as a metallopeptidase coded by the gene DR_2310, and band 3 (B3) was identified as a 5′-nucleotidase protein coded by the gene DR_0505. The remaining three bands (B4, B5, and B6) were identified as proteins coded by a pool of three genes associated with the same operon, and they are named DR_A0283,

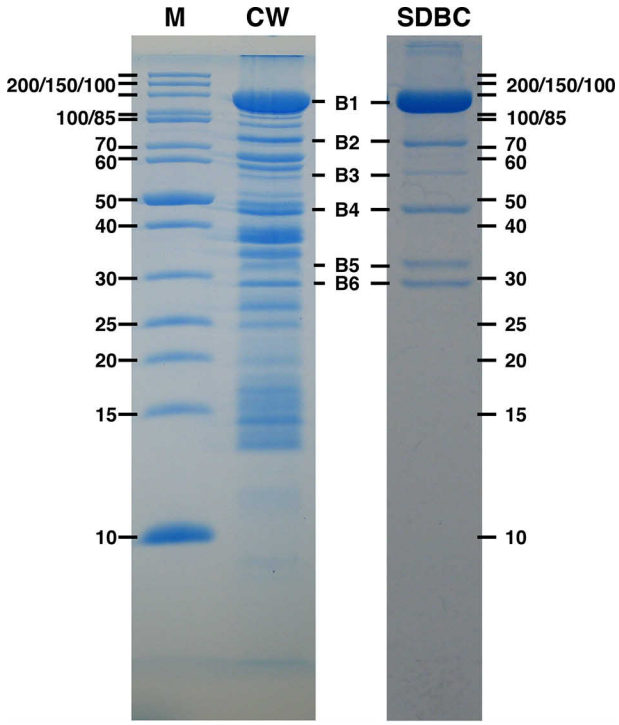

Figure 2. SDS-PAGE of the isolated samples: cell wall fragments and SDBC. *Lane CW* (cell walls) shows a typical pattern of bands from the isolated cell wall fragments shown in Fig. 1; *lane SDBC* shows the typical pattern of bands constituting the main SDBC pool isolated by SEC. This sample results in a heavier dominant band (*B1*) and five less-represented bands (from *B2* to *B6*); the equivalence of each SDBC band in the cell wall samples is also shown. *Lane M* indicates the protein standard and the respective molecular weights; the level and mass of each marker band is also indicated on the *right side* of the *SDBC lane*. The *dashes* show the correspondence between the components of the cell wall fragments and those of the SDBC.

DR_A0282, and DR_A0281. Among these operonic genes, only the DR_A0283, a probable subtilase-type serine protease, has an assigned function, and the remaining two are uncharacterized proteins having similarity with peptidases (Table 2). Taken together, the MS analysis suggested the SDBC minor subunits to be related to the processing of complex substrates (*e.g.* proteins) before their transport as simple units (*e.g.* amino acids).

SDBC is a channel with peculiar gating properties

To evaluate its pore-forming ability, we have reconstituted the SDBC into lipid bilayer membranes composed of 1,2-diphytanoyl-*sn*-glycero-phosphatidylcholine (DPhPC). Preliminary tests performed in 1 M KCl indicated that the SDBC forms highly conductive channels (~10–20 nS; data not shown). Hence, we have chosen to study these channels at an ion concentration of 100 mM. Sufficient membrane current increments (ΔI_m) due to channel insertions were observed under three types of electrolyte solutions (KCl, LiCl, and CH_3COOK) and allowed to calculate the SDBC conductance at a membrane potential (V_m) of 20 mV ($\Delta G_{SDBC} = \Delta I_m/V_m$; Figs. 5 and 6). The calculated minimum conductance and the related total number of channel insertions were both estimated as indicated in Table 3. In some cases, channel insertion rates were rapid, reaching a total membrane current of ~100 pA (Fig. 5, *insets*), whereas in LiCl the amount of total insertions and their rates were found to be much lower (Fig. 5).

At times, the inserted channels showed a behavior of a fast flickering gating to a lower conductance state (Fig. 6). The gating-related conductance for these cases is indicated in Table 3. By observing the step increments associated with channel insertions, it emerges that the SDBC does not have a well-defined state. In fact, stepwise insertions yielded an increase in the membrane current mostly ranging from ~5–6 to ~50–60 pA, which corresponds to a conductance of ~0.25–0.30 to ~2.5–3.0 nS, for all the electrolyte species studied (Fig. 7).

Information about the single SDBC unit conductance was obtained from a pool of more than 100 channel insertions (Fig. 7). As shown in the histograms of Fig. 7, the SDBC conductances are widely distributed for all three electrolyte solutions (binning ~0.25–0.30 nS).

SDBC is a nonselective channel

Next, we have investigated the ion selectivity of the SDBC by measuring the reversal potential (V_{rev}). A lipid bilayer was formed and kept in contact with a 100 mM salt solution on both sides of a bilayer carrying a multitude of channels. In these conditions, a current–voltage (I–V) recording of this multichannel state was captured by varying the V_m values from +50 to −50 in decrements of ΔV_m = 10 mV, and its profile was treated as the blank (no salt gradient). Subsequently, identical I–V measurements were performed while changing the salt concentration on one side of the membrane with constant increments (Δ[salt] = 100 mM). The reversal potential was determined by comparing this I–V profile with that of the blank. The V_{rev} values at different electrolytes concentrations (KCl, LiCl, and CH_3COOK) were plotted and compared (Fig. 8). The V_{rev} is described according to the Goldman-Hodgkin-Katz (GHK) Equation 1, where the selectivity of the channel is expressed as the ratio of the permeabilities of the anion and the cation (P_{C+}/P_{A-}).

$$V_{rev} = \frac{RT}{F}\ln\left(\frac{P_C[C^+]_{out} + P_A[A^-]_{in}}{P_C[C^+]_{in} + P_A[A^-]_{out}}\right) \quad \text{(Eq. 1)}$$

The permeability ratios reflect the effective mobilities of the ions inside the channel (μ^c). Accordingly, for an ion-selective channel, the permeability ratio is expected to be different from the ratio of the bulk mobilities (μ^b_{C+}/μ^b_{A-}) of the ions (47). For KCl, a permeability ratio of ~1.06 (P_{K+}/P_{Cl-} = 1:0.94) was obtained, which indicates a rather nonselective channel (μ^b_{K+}/μ^b_{Cl-} = 1:1). It is worthy to note that the permeability ratios obtained for LiCl, ~0.53 (P_{Li+}/P_{Cl-} = 1:1.86), and for CH_3COOK, ~1.67 (P_{K+}/P_{CHCOO-} = 1:0.6), directly reflect the ratios of the corresponding bulk mobilities of these ions; hence, it can be concluded that the channels are nonselective.

Discussion

The results described here challenge the previous mono-protein model for this S-layer (21). In particular, they confirm and reinforce a new model in which the S-layer structural units are composed of several proteins and integrated with the entire bacterial cell wall (33). The main architectural unit is composed of a planar hetero-oligomeric complex where the protein DR_2577 is the primary component. This protein was previ-

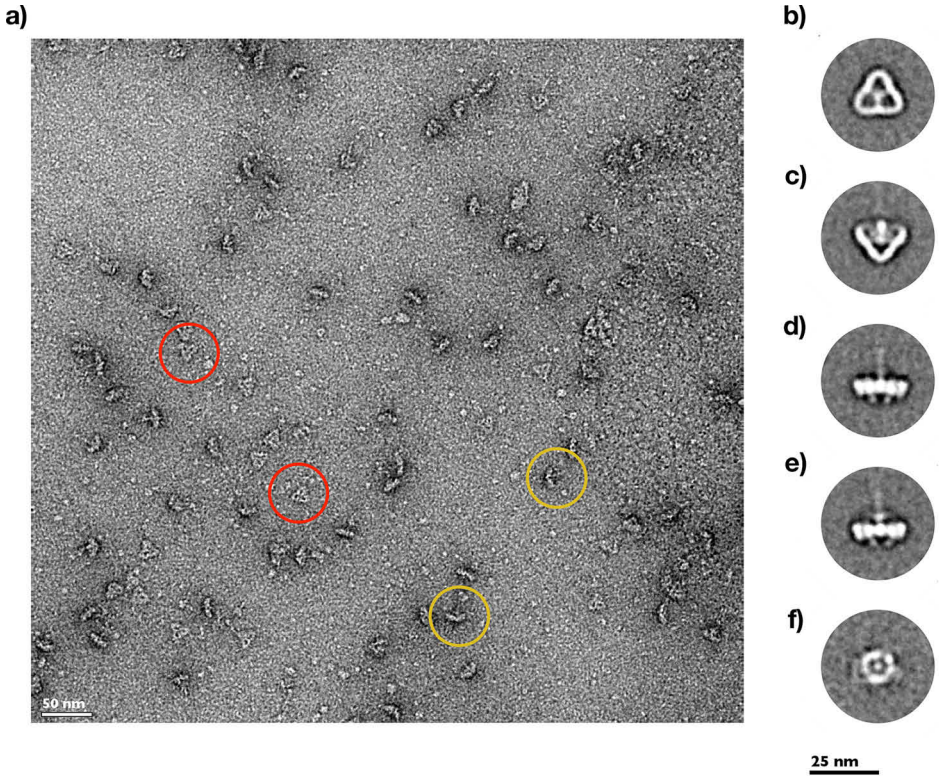

Figure 3. Electron micrographs and selected 2D class averages of the SDBC. The SDBC sample appears homogeneously composed of a single particle that can be appreciated in different orientations (*a*). Particles delimited by the *yellow circles* show typical side views, and particles in the *red circles* show typical top views of the SDBC. Detail of the SDBC particle observed from a top view (*b*), from a partially tilted side view (*c*), from a side view (*d* and *e*), and finally from a bottom view (*f*) is shown. *Scale bars* are indicated.

Table 1
Molecular weight of the SDBC
The molecular weight of the SDBC was estimated by two different methods.

Method	Estimated mass
	kDa
Size-exclusion chromatography[a]	>750
BN-PAGE[a]	~800

[a] Data were calculated according to Farci *et al.* (36).

ously shown to be organized into homohexameric complexes based on trimeric assemblies of stable dimers (36), and it was found to have an essential role in the formation and stability of this S-layer (11, 12, 35). Moreover, the binding of the carotenoid cofactor deinoxanthin to DR_2577 has been shown to protect *D. radiodurans* from UV radiation, especially under desiccation conditions, and to confer thermostability, eventually highlighting the functional relevance of DR_2577 on this S-layer (11, 12). In this work, the SDBC was isolated in presence of a mild detergent in low concentrations. These soft conditions allowed the retention of several minor subunits, previously not detected (36) and here identified as coded by the genes DR_2310, DR_0505, DR_A0281, DR_A0282, and DR_A0283 (Table 2). Although for two of these subunits, DR_A0281 and the DR_A0282, the function is unknown but showing similarity with peptidases, the DR_A0283 is identified as a probable subtilase-type serine protease; accordingly, these three proteins appear as essential components for chopping proteins into amino acids, suggesting a possible auxiliary role for the SDBC function. Moreover, the proteins DR_0505, a 5′-nucleotidase, and the DR_2310, a metallopeptidase, were previously identified as part of the DNA Processing Complex (33, 48), also suggesting an ancillary role for the SDBC function of transport across the outer membrane. The present procedure allows us to isolate an SDBC retaining its auxiliary subunits, while only the isolation of DR_2577 hexamers was previously reported (36). These differences cannot be simply explained in terms of mildness of the procedure used here with respect to the one previously described. In fact, the latter was performed in absence of detergents; hence, the extraction was not chemically based but was physically based by using a French pressure cell, letting only the most hydrophilic fraction pass in solution, which was only composed of DR_2577 hexamers (36). Here, the whole isolation is performed in the presence of the mild detergent β-DDM, and during the solubilization of cell wall fragments also the most hydrophobic components are solubilized and retained by the SDBC (*e.g.* the auxiliary subunits).

In EM the cell wall of *D. radiodurans* appears as a single dense structure around 30 nm thick, which includes a layer of sugars, the S-layer, the outer membrane, the periplasm, and the inner membrane (21). In this context is placed the SDBC that, inclusive of its auxiliary subunits, exhibits a triangle-like structure with an apparent 3-fold symmetry delineated by three pores (Fig. 3). This structural feature is typically observed in porins such as Omp, Opr (outer membrane porin), the outer membrane receptor, and others (42). Each SDBC particle had a triangular shape with a 20-nm side and ~3.5-nm height, suggesting that this complex does not span both membranes, but it is rather limited to the outer membrane, further hinting for porin-related structural properties. However, this complex was

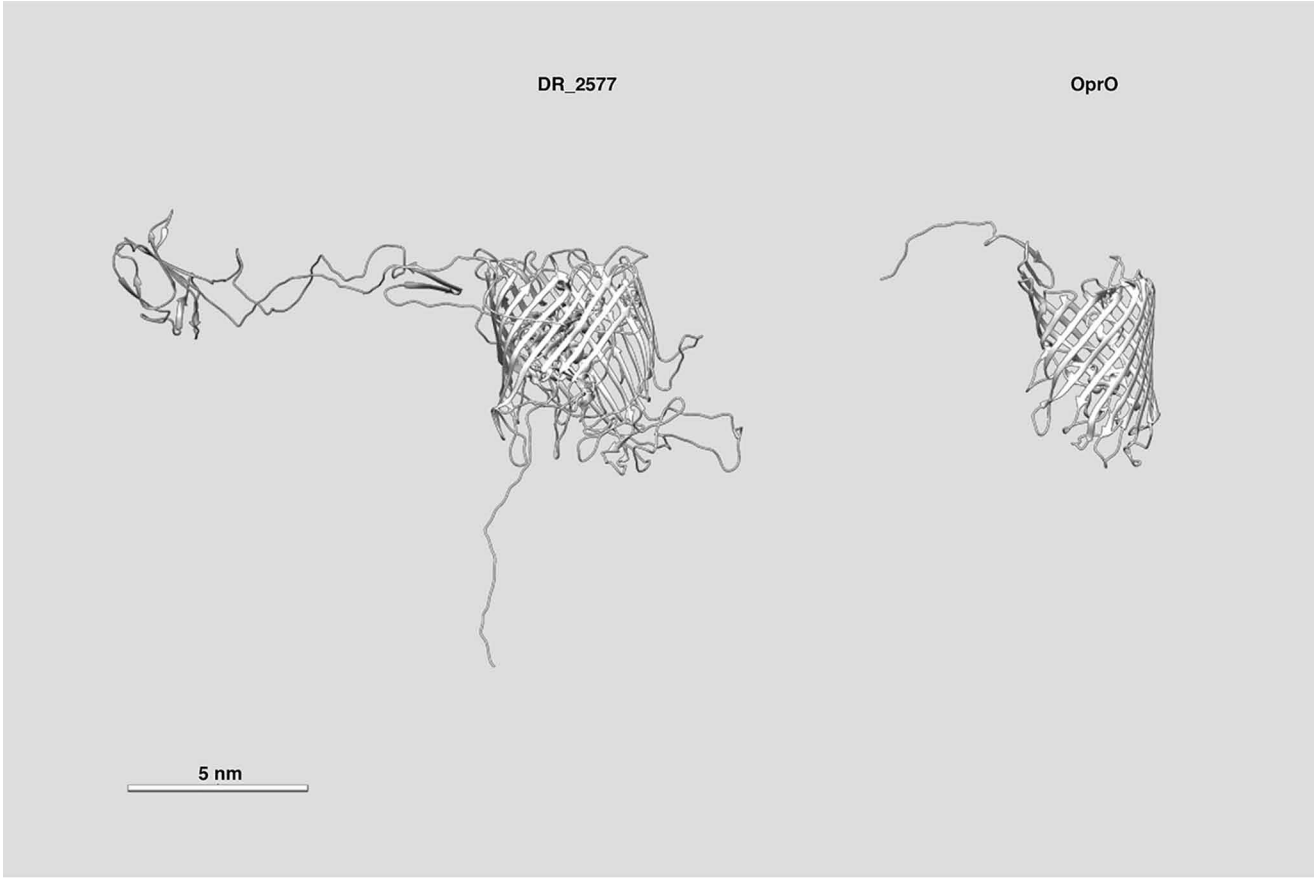

Figure 4. Comparison between the predicted structure of the DR_2577 and the OprO from *P. aeruginosa*. Whereas the size of the two proteins is extremely different, a visual comparison of their structure recalls a similar tertiary organization. The side view for the two structures is shown. The *scale bar* is reported on the image.

Table 2
SDBC subunit composition identified by MS
Mass spectrometry analysis performed on the bands resolved by SDS-PAGE of the pure SDBC. The analysis identified the main protein subunits of this complex.

SDS-PAGE band	Gene	Uniprot identifier	Mass	iBAQ score	Protein name	Function and properties	
			kDa				
B1	DR_2577	Q9RRB6	124	$3.81e^{+10}$	S-layer protein A (SlpA)	Carotenoid-binding protein	UVC/UVB protection (Farci *et al.* (11)); thermostability (Farci *et al.* (12)); porin (this study)
B2	DR_2310	Q9RS17	84	$1.18e^{+10}$	Uncharacterized protein	Probable metallopeptidase	DPC proteins–DNA processing (Kota and Misra (48) and Farci *et al.* (33))
B3	DR_0505	Q9RX10	60	$4.70e^{+9}$	5′-nucleotidase family protein	Nucleotidase	
B4	DR_A0283	Q9RYM8	77	$7.80e^{+9}$	Probable subtilase-type serine protease	Probable peptidase	Operon with unknown function (Farci *et al.* (33))
B5	DR_A0282	Q9RYM9	55	$6.71e^{+9}$	Uncharacterized protein	Probable peptidase[a]	
B6	DR_A0281	Q9RYN0	11	$1.42e^{+10}$	Uncharacterized protein	Probable peptidase[a]	

[a] Possible function was inferred from blast analysis.

found to be 4–7 times bigger than a typically-known porin and has a characteristic needle-like structure departing from its center, which may appear bent in some particles (Fig. 3, *c–e,* and Fig. S2). This structure may possess the essential function of hooking the above-placed layer of sugars. According to the well-known structure–function relationship of proteins (49), structural features hinting at the possible porin-like function associated with the SDBC were also tested and confirmed by bioinformatic analyses. Given that minor auxiliary subunits contribute to the complex for ~27% with respect to both amino acid sequences and molecular mass, the only DR_2577 primary structure was analyzed for sequence and structural similarity against well-characterized porins such as Omp38 and OprO from the S-layer–carrying bacteria *A. baumannii* and *P. aeruginosa*, respectively. This analysis showed that the core of the DR_2577 sequence is the hot spot of the similarity. This region of the primary sequence contains the typically-conserved sites related to the function of porins (Fig. S3) and has their characteristic secondary structure (42). Moreover, the structural homology model for this region strictly matches with previous studies assigning to it a β-barrel structure (12, 37). It has to be emphasized that S-layer proteins are the result of recombination events (38, 39, 40); thus, except for their SLH domain (38), they are characterized by highly-variable struc-

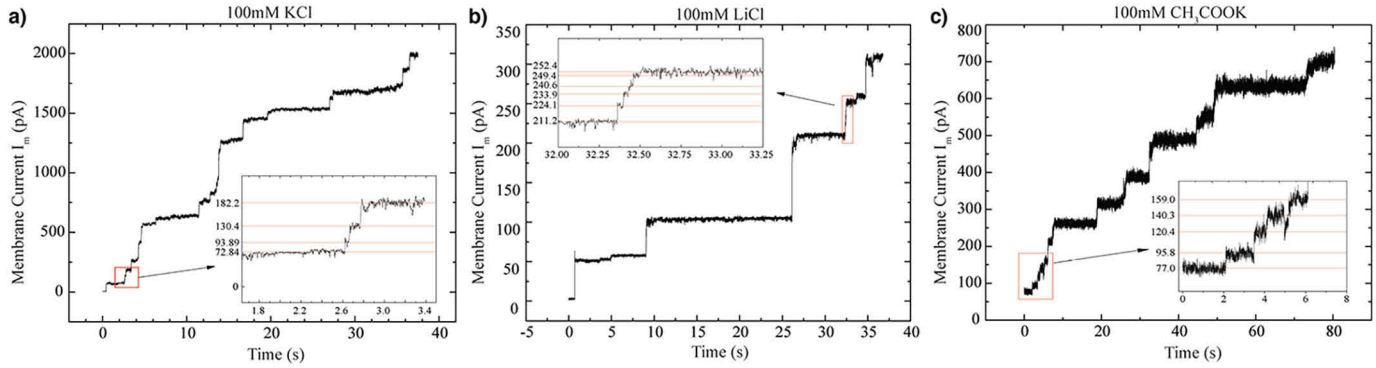

Figure 5. Stepwise insertions of the SDBC. Stepwise increases of membrane current at a membrane potential of 20 mV. Stepwise insertions of the SDBC in 100 mM of KCl (*a*), LiCl (*b*), and CH_3COOK (*c*) are shown. *Insets* show the detail where fast insertions are resolvable and where insertions with varied conductances are observed. The signals were filtered at 1000 Hz.

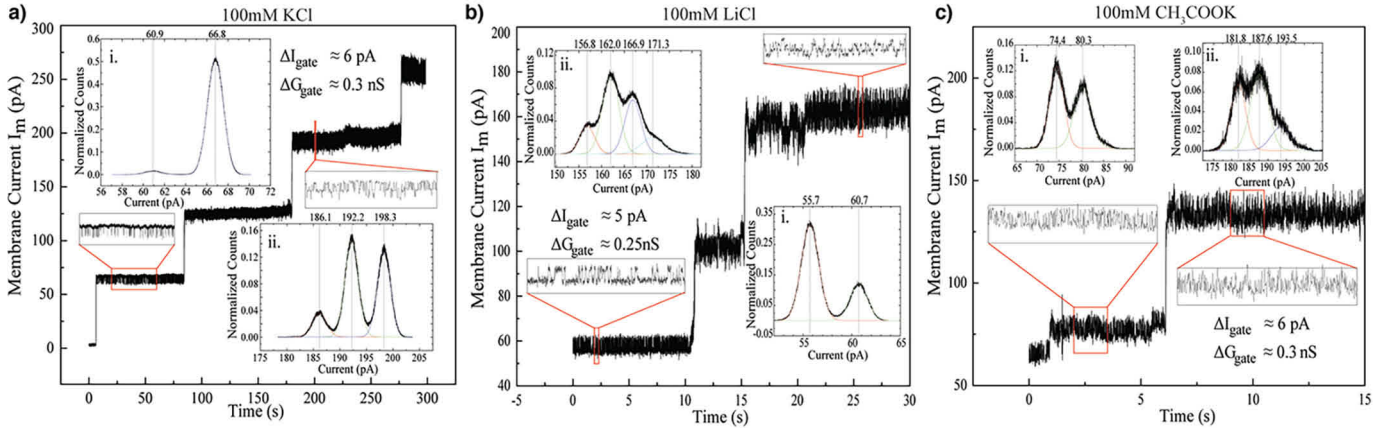

Figure 6. Gating states of the SDBC. Segments of current traces from multiple channel insertions and related gating behavior at 100 mM concentrations of KCl, LiCl, and CH_3COOK are shown. Channel insertions, gated states, and their detail are depicted for KCl (*a*), LiCl (*b*), and CH_3COOK (*c*). For all subfigures, *insets i* and *ii* show the current histograms for the lower and higher conductance states, respectively. The histograms are areas normalized and fit to Gaussians to distinguish the sub-gated states. The signals are filtered at 1000 Hz.

Table 3

Channel conductance estimated for the SDBC

The minimum conductance and the related total number of channel insertions are shown. See text for the interpretation of gating.

Electrolyte	Minimum unit of conductance[a]	Estimated conductance from gating[b]	Ion selectivity (P_{anion})	Total no. of channel insertions analyzed
	nS	*nS*		
KCl	0.3	3	0.94	269
LiCl	0.25	2.5	1.86	158
CH_3COOK	0.3	3	0.6	310

[a] Channel conductance was estimated from the minimal unit of conductance observed.
[b] Channel conductance was estimated from the gating pattern of the channel insertions.

tures and functions, allowing the presence of domains that are species-specific either for basic physiological functions (*e.g.* exchanges with the environment) or for unique resistance properties (*e.g.* defense against adverse environmental conditions or invasion of a host) (4, 11–15). Accordingly, we can assume that the similarity between the DR_2577 and the two porins mentioned above is a true hint toward the functionality of the SDBC and thus of this specific S-layer. If we compare the SDBC with widely-studied porins, it can be noticed that they show a characteristic conductance of ~1–4 nS, in 1 M KCl, as well as a sharp distribution around their single-channel conductance in multichannel insertion assays (50, 51), properties that are not present in the SDBC. Differently, the striking SDBC feature is that its conductance distribution is quite large even though the minimal conductance (G_m) step is assumed to be the single-channel conductance at 100 mM electrolyte concentration (*e.g.* $G_m \approx 0.25$ nS; Fig. 6).

Considering the previously described DR_2577 structure (Fig. 4) (12, 37), and the small weighted contribution of the auxiliary subunits in the SDBC, the DR_2577 hexamer can be identified as the main contributor to the SDBC pore regions (Fig. 3*b*). Furthermore, considering that a DR_2577 hexamer results from an assembly of three stable dimers (36), we can hypothesize that each DR_2577 dimer contributes to a single pore. Consequently, it is natural to look for the dimer as a singular unit conductance (G_i) in multiples of three (G_i:$3G_i$:$3nG_i$). However, only a heterogeneous pattern in conductance was observed (Fig. 7). This behavior was attributed to the self-assembling properties of the SDBC; thus, given the measured $G_m \approx 0.25$ nS, the singular unit conductance should sit within 0.25 and 0.5 nS.

Interestingly, in some signal recordings, a fast-flickering gating behavior of the SDBC can be observed (Fig. 6) in conjunction with an almost uniform stepwise increment per channel insertion ($\Delta I^{mKCl} = \Delta I^{mCH3COOK} \approx 60$ pA and $\Delta I^{mLiCl} \approx 50$ pA).

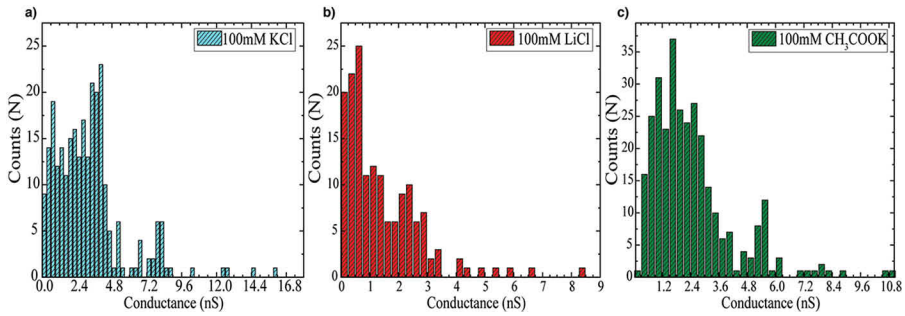

Figure 7. Distributions of channel conductance. Channel conductances were obtained by analysis of stepwise increments. Membrane currents with three different electrolyte solutions were measured. Distributions for KCl (*a*), LiCl (*b*), and CH_3COOK (*c*) are shown. For KCl and CH_3COOK, the data are binned at 0.3 nS and for LiCl at 0.25 nS.

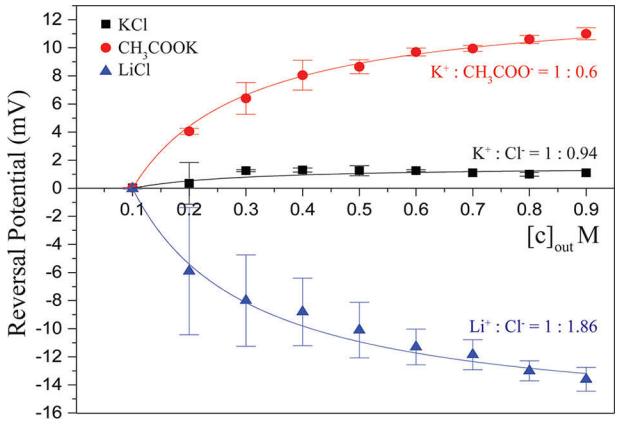

Figure 8. Reversal potential curves of SDBC channels for three different salt species. *Black boxes* represent KCl, *red circles* represent CH_3COOK, and *blue triangles* represent LiCl. The lines are fits to the GHK Equation 1.

As more channels are inserted, more sub-states are distinctly separated by a specific conductance as evidenced in Fig. 6*a* (*insets i* and *ii*).

After the first and second insertions, current traces in KCl are characterized by a fast-flickering conductance state where the current trace fluctuates by 6 pA. However, after the third channel insertion, the trace shows a fast-flickering state with two distinct sub-states separated by 6 pA. Traces of recordings performed in CH_3COOK show a similar behavior, whereas in the case of LiCl, these substrates are separated by a fluctuation of 5 pA (Fig. 6*a*, *insets i* and *ii*). Within the light of this information, it can be concluded that a single functional SDBC unit has a large open channel conductance state with a sub-gated state of $\Delta G_{KCl}{}^{gate}$, $\Delta G_{CH3COOK}{}^{gate} = 0.30$ nS and $\Delta G_{LiCl}{}^{gate} = 0.25$ nS, and as more channels are inserted, it is possible to distinguish more of these particular substrates. This fact would indicate that if a trace with one sub-conductance state describes a single channel, then a state with two sub-conductance states describes two channels and so forth. Accordingly, the single-channel conductance of an SDBC unit is $G_{SDBC}{}^{KCl} = G_{SDBC}{}^{CH3COOK} \approx 3$ nS and $G_{SDBC}{}^{LiCl} \approx 2.5$ nS; alternatively, given the similarity between the conductance magnitude drop due to the flickering events (Fig. 6) and the lowest amount of conductance observed by channel insertions (Fig. 6, *e.g.* $\Delta G^{gate} \approx G_{min}$), the flickering can be assumed as caused by the complete gating (closure) of a single unit of the SDBC. As more channels are inserted in the bilayer, more of these completely gating channels are encountered, and hence the single-channel conductance of an SDBC unit is $G_{SDBC}{}^{KCl} = G_{SDBC}{}^{CH3COOK} \approx 0.3$ nS and $G_{SDBC}{}^{LiCl} \approx 0.25$ nS. However, considering the relevance of the SDBC self-assembling properties and the stepwise insertions data here shown, it is more likely that the smaller conductance steps reflect the unit conductance and that the higher conductance levels result from insertions of SDBC higher oligomeric assemblies.

Finally, the reversal potential measurements indicate that the channel is nonselective in relation to the large channel conductances (Table 3). The extent to which the charges are screened by a channel primarily depends on four factors: (i) the amount and strength of the surface charges on the channel; (ii) the size of the channel lumen where the bulk flow of ions occurs; (iii) the presence of constriction zones within the channel; and (iv) the concentration of ions in solution. At room temperature, for a monovalent electrolyte species the Debye-Length (λ_D), a measure expressed in nanometers of screened charged surfaces distance, is given by λ_D (nm) $= 0.304/[M]^{1/2}$. Being $[M]$ the molar concentration of the electrolyte (100 mM), it results that $\lambda_D \approx 1$ nm. From the experimental conductance, we can evaluate the dimension of the pore assuming a simple diffusion process, in agreement with the low selectivity measured. From Ghai *et al.* (52), we applied the extracted equation P = D/L to calculate P, the permeability coefficient (nm/ns), by using the diffusion constant D for ions (D = 3 nm^2/ns) and the geometrical length of the channel (L = 3.5 nm), finally estimating a radius range 0.4 nm $<$ R $<$ 1.2 nm. Hence, our results suggest that the channel lumen is larger than OmpF or OprO (0.3 nm $<$ R $<$ 0.5 nm) (46, 52) with the possible presence of weak surface charges on the channel.

In *D. radiodurans,* the continuity of self-assembled SDBC units forming the characteristic S-layer organization is an essential requirement for its fitness (11, 12, 35). However, the mechanism by which such a continuous proteinaceous barrier is also able to ensure permeability and allow the passage of nutrients has never been addressed. The reported SDBC findings present the S-layer not only as a defensive barrier providing the specific resistance capabilities of this bacterium, but also as a "breathing membrane" allowing the normal exchange of substances in/out of the cell. There are increasing evidences for large protein complexes forming integral parts of cell envelopes from both eubacteria and archaebacteria (53–56). Accordingly,

because S-layers have been identified in a large number of bacterial species, it would be interesting to speculate whether in other organisms they also contain large complexes as main constituents and, if so, whether these complexes carry one or more specific functions of resistance together with the functions of permeability.

In this context, it is important to highlight that pathogenic bacteria, such as *Bacillus anthracis* (57, 58), *Helicobacter pylori* (59), *Yersinia pestis* (60), *Campylobacter fetus* (61), and many others, contain S-layers that are essential components in adhesion of bacterial cells to their hosts and in their resistance to extreme conditions (57, 58, 61). In particular, it is worth mentioning the case of *A. baumannii,* the Omp of which improves the adhesion to the host contributing to its high infectivity and its increasing antibiotic resistance. Both these properties are strictly related to the low permeability of its outer membrane (15, 62). This fact implies that a proper understanding of the S-layer architecture will be important for developing new strategies against these pathogens.

The multiple functionality of the SDBC and its peculiar properties suggests a much more complex machinery involved in the physiology of this S-layer. In biology, structural models occurring in highly-repeated units are always related to a functional specialization. In this system, so far, it can be appreciated that the only resulting functional output are the gating properties; however, the primary functional reason of this organization still remains unclear. Further studies will follow to find greater details about the structure and function of this system to finally unveil what remains hidden from us by nature.

Experimental procedures

Bacterial strain and growth conditions

D. radiodurans strain R1 (ATCC 13939) was grown in tryptone/glucose/yeast extract broth (TGY) (63) for 24 h at 30 °C, with shaking at 250 rpm. Cells were harvested by centrifuging the bacterial cultures at 5000 × *g* for 10 min at 4 °C and resuspended in buffer A (50 mM Na phosphate, pH 7.8).

Membrane preparation

Whole-cell membrane fractions were purified at 4 °C according to Farci *et al.* (33). Cells were resuspended in buffer A, treated with DNase, and disrupted using a French pressure cell. Unlysed cells were removed by low-speed centrifugation (4 °C, two times at 2000 × *g* for 10 min). The final supernatant was centrifuged again (4 °C, 48,000 × *g* for 10 min), and the pink pellet, consisting of cell walls fragments, was resuspended in 10 ml of buffer A. To remove surface polysaccharides, the membrane suspension was incubated under agitation (800 rpm) with 100 μg/ml lysozyme for 8 h at 30 °C. The membrane suspension was then washed three times in buffer A by cycles of resuspension/centrifugation (4 °C, 48,000 × *g* for 10 min).

Membrane solubilization

Before the final resuspension, cell wall fragments were weighed. The mass of the cell wall fragments fraction was assumed to be the total protein mass. The measured mass was used for calculating the detergent concentration for solubilization. Cell wall fragments were solubilized by agitation in 1% (w/v) β-DDM at room temperature for 3–4 h with a final protein concentration of 3–5 mg/ml. The solution was then centrifuged at 48,000 × *g* at 10 °C for 10 min to remove insoluble material.

SDBC isolation

The supernatant obtained was processed by two stages of chromatography. The solubilized sample was injected on an anion-exchange chromatography column (Hiload HP, GE Healthcare, Uppsala, Sweden) equilibrated in buffer B (50 mM Na phosphate, pH 7.4, 0.05% (w/v) β-DDM), and after a step of binding and washing, the bound components were eluted in a gradient of 0–100% buffer C (50 mM Na phosphate, pH 7.4, 2.5 M NaCl, 0.05% (w/v) β-DDM). The SDBC fractions were first identified by their typical pink color and, subsequently, by denaturing electrophoresis. Next, the SDBC pool was concentrated using a Vivaspin 20 ultrafiltration membrane with a 100-kDa cutoff (GE Healthcare). The obtained sample was loaded on a Superose 6 column (Superose 6 10/300GL, GE Healthcare) previously equilibrated in its mobile phase (buffer B). Whole equilibrations and the runs were performed at a flow rate of 0.5 ml/min. The molecular weight of the SDBC complex resolved by the size-exclusion chromatography was estimated as reported previously (36).

Bioinformatic analysis

The Universal Protein Knowledgebase (UniProt) server (**RRID:SCR_002380**) (64, 65) was used for obtaining the DR_2577 (Q9RRB6), the Omp38 (Q6RYW5), and the OprO (P32977) sequences. The HHpred software from the Toolkit in the Tübingen suite was used for blind protein homology detection based on sequence and structurally accurate prediction, and the Clustal Omega tool from the same suite was used for sequence alignment (RRID:SCR_010276) (66–69). The structural prediction was done by using the RaptorX suite (RRID:SCR_018118) (70). Molecular graphics images were produced using the UCSF Chimera package from the Resource for Biocomputing, Visualization, and Informatics at the University of California, San Francisco (71).

PAGE

For denaturing SDS-PAGE, 10% (w/v) separating polyacrylamide/urea gels with 4% (w/v) stacking gels were used (72). Samples were denatured with Rotiload (Roth) at room temperature before loading, and after the electrophoretic separation, the gels were stained with Coomassie Brilliant Blue G-250. Blue Native (BN) gel electrophoresis was carried out using 3–12% (w/v) continuous gradient gels (36, 73). The cell wall fragments were mixed with 0.25 volume of Coomassie Blue Solution 5% (v/v), Serva Blue G, 750 mM aminocaproic acid, and 35% (w/v) sucrose. Electrophoresis was carried out at 205 V for 5 h at 4 °C. The molecular weight of the SDBC complex resolved by BN-PAGEs was estimated as reported previously (36).

Electron microscopy and data processing

Five microliters of purified SlpA complexes in solution was applied to copper EM grids (EMS200-Cu) covered with a 20-nm carbon film, which were glow-discharged for 30 s with a 5-mA current before specimen application. Excess sample was removed after 1 min by blotting (Whatman No. 1 filter paper) for 1- 2 s, and the grid was immediately stained with 5 μl of 2% uranyl acetate for 1 min and blotted to remove excess stain. A large data set of optimized and negatively-stained specimen grids was acquired with a Tecnai F20 microscope (Thermo Fisher Scientific) operating at an accelerating voltage of 200 kV, with a FEI Eagle 4K CCD camera, at a magnification of 72,539 ss× and a pixel size of 1.93 Å. Altogether, 564 micrographs were acquired with defocus ranging from 2 to 5 μm. After quality inspection and determination of contrast transfer function parameters with the GCTF program (74), micrographs were subjected to particle picking. Approximately 87,312 particles were semi-automatically picked with the e2boxer.py routine of the EMAN2 program (75) and subjected to five rounds of 2D classification using Relion 1.4 (76), with 3× 120, 80, and 20 classes, respectively, which reduced the data set to 29,414 particles. All 2D classifications comprised 25 iterations, and no symmetry was imposed. The presented resolution of the class averages corresponds to the lowest signal-to-noise ratio (SNR) value (≥1) indicated in the *model.star file and the resulting output from the last iteration of the final 2D classification. The number of particles contributing to the class averages was also found in the *model.star files.

Mass spectrometry

Protein identification by mass spectrometry from bands in SDS-PAGE was essentially performed as described in Haniewicz *et al.* (77). Briefly, bands of interest were subjected to in-gel digestion after reduction (with DTT) and alkylation (with iodoacetamide) using sequencing-grade modified trypsin. Extracted peptides were analyzed by LC-MS/MS using a nanoAcquity UPLC system (Waters) coupled to an Orbitrap Fusion Lumos (Thermo Fisher Scientific) mass spectrometer. Data analysis was performed with the software MaxQuant (version 1.5.3.28) (78), and raw files from the MS were searched using the Andromeda search engine (79) against a species-specific Uniprot database (*D. radiodurans*, June 2019, 3120 entries) with a list of common contaminants appended. The mass error tolerance for the full scan MS spectra was set at 20 ppm and for the MS/MS spectra at 0.5 Da. Trypsin specificity (no cleavage if Lys/Arg followed by Pro) was used for the search, with a maximum of two missed cleavages allowed. The search included the following modifications: carbamidomethyl (cysteine, fixed), oxidation (methionine, variable), and N-terminal acetyl (protein, variable). A filter of an Andromeda score of 40 for a protein to be identified was applied. Peptides and protein hits were filtered at a false discovery rate of 1% using a target-decoy strategy (80). No proteins are reported with fewer than two peptides per protein in at least one of the bands (Table S1). The intensity-based absolute quantification (iBAQ) values were used to determine the most abundant protein per gel band from the analysis.

Electrophysiology assays

Channel recording apparatus consisted of a two-compartment Teflon chamber (~2.5 ml each) separated by a 25-μm–thick Teflon partition with an aperture of diameter ~100 μm for membrane formation. Bilayer lipid membranes were formed from DPhPC using the monolayer opposition technique (81). The aperture was pretreated with a hexadecane/hexane solution (1% v/v) and left for ~20 min to achieve solvent evaporation. The *trans*- and *cis*-sides of the chambers were filled with buffer solution (100 mM KCl, 10 mM HEPES, pH 7.0), and 10 μl of lipid in pentane (5 mg/ml) was added to both sides of the chamber allowing bilayers to form. Channel reconstitution was achieved by the addition of purified SDBC into the *cis*-side of the chamber. A volume of 0.5 μl of SDBC stock solutions (1 mg/ml) was diluted ~10^5 times by a solution of Genapol (1.1% v/v). Channel current traces were recorded with Ag/AgCl electrodes in agarose salt bridges containing 3 M KCl or with calomel electrodes containing a salt bridge (Metrohm AG) in the case of reversal potential measurements. The *cis*-side of the chamber was considered the virtual ground, and measurements were done using the Axopatch 200B (Molecular Devices, LLC) patch-clamp amplifier in V-clamp mode (whole-cell $\beta = 1$) with a CV-203BU headstage. The output signal was filtered by a low-pass Bessel filter at 10 kHz and saved at a sampling frequency of 50 kHz using an Axon Digidata 1440A digitizer (Molecular Devices, LLC). Data analysis was performed with Clampfit 11.0.3 (Molecular Devices, LLC) and Origin Lab 2018 (Northampton, MA). For acquisition and analysis of reversal potential measurements, a homemade LabVIEW (National Instruments) was used.

Data availability

The mass spectrometry proteomics data have been deposited to the ProteomeXchange Consortium via the PRIDE (84) partner repository (82, 83) with the dataset identifier PXD015568.

Author contributions—D. F., M. A. A., I. B., and D. P. conceptualization; D. F., M. A. A., I. B., M. C., J. K., M. W., S. K., and D. P. data curation; D. F., M. A. A., S. F. F., J. A. B., I. B., M. C., J. K., S. K., and D. P. formal analysis; D. F., S. K., and D. P. funding acquisition; D. F., M. A. A., J. A. B., I. B., M. C., M. W., S. K., and D. P. validation; D. F., M. A. A., S. F. F., J. A. B., I. B., M. C., J. K., S. K., and D. P. investigation; D. F., M. A. A., J. A. B., I. B., M. C., M. W., S. K., and D. P. visualization; D. F., M. A. A., I. B., M. C., J. K., M. W., S. K., and D. P. methodology; D. F., M. A. A., J. A. B., I. B., M. C., J. K., M. W., S. K., and D. P. writing-original draft; D. F., M. A. A., I. B., M. C., J. K., M. W., S. K., and D. P. writing-review and editing; D. P. supervision; D. P. project administration.

Acknowledgments—The Fritz Lipmann Institute is a member of the Leibniz Association and is financially supported by the Federal Government of Germany and the State of Thuringia. We gratefully acknowledge support from the Fritz Lipmann Institute Core Facilities Proteomics.

References

1. Sleytr, U. B. (1975) Heterologous reattachment of regular arrays of glycoproteins on bacterial surfaces. *Nature* **257,** 400 – 402 CrossRef Medline

2. Sleytr, U. B. (1978) Regular arrays of macromolecules on bacterial cell walls: structure, chemistry, assembly, and function. *Int. Rev. Cytol.* **53,** 1–62 CrossRef Medline
3. Messner, P., and Sleytr, U. B. (1991) Bacterial surface layer glycoproteins. *Glycobiology* **1,** 545–551 CrossRef Medline
4. Sleytr, U. B., Messner, P., Pum, D., and Sára, M. (1993) Crystalline bacterial cell surface layers. *Mol. Microbiol.* **10,** 911–916 CrossRef Medline
5. Bahl, H., Scholz, H., Bayan, N., Chami, M., Leblon, G., Gulik-Krzywicki, T., Shechter, E., Fouet, A., Mesnage, S., Tosi-Couture, E., Gounon, P., Mock, M., Conway de Macario, E., Macario, A. J., Fernández-Herrero, L. A., *et al.* (1997) Molecular biology of S-layers. *FEMS Microbiol. Rev.* **20,** 47–98 CrossRef Medline
6. Messner, P., Allmaier, G., Schäffer, C., Wugeditsch, T., Lortal, S., König, H., Niemetz, R., and Dorner, M. (1997) Biochemistry of S-layers. *FEMS Microbiol. Rev.* **20,** 25–46 CrossRef Medline
7. Pavkov, T., Egelseer, E. M., Tesarz, M., Svergun, D. I., Sleytr, U. B., and Keller, W. (2008) The structure and binding behavior of the bacterial cell surface layer protein SbsC. *Structure* **16,** 1226–1237 CrossRef Medline
8. Gentner, N. E., and Mitchel, R. E. (1975) Ionizing radiation-induced release of a cell surface nuclease from *Micrococcus radiodurans*. *Radiat. Res.* **61,** 204–215 CrossRef Medline
9. Sleytr, U. B., and Sára, M. (1997) Bacterial and archaeal S-layer proteins: structure–function relationship and their biotechnological applications. *Trends Biotechnol.* **15,** 20–26 CrossRef Medline
10. Pavkov-Keller, T., Howorka, S., and Keller, W. (2011) The structure of bacterial S-layer proteins. *Prog. Mol. Biol. Transl. Sci.* **103,** 73–130 CrossRef Medline
11. Farci, D., Slavov, C., Tramontano, E., and Piano, D. (2016) The S-layer protein DR_2577 binds the carotenoid deinoxanthin and under desiccation conditions protect against UV-radiation in *Deinococcus radiodurans*. *Front. Microbiol.* **7,** 155 CrossRef Medline
12. Farci, D., Slavov, C., and Piano, D. (2018) Coexisting properties of thermostability and Ultraviolet radiation resistance in the main S-layer complex of *Deinococcus radiodurans*. *Photochem. Photobiol. Sci.* **17,** 81–88 CrossRef Medline
13. Beveridge, T. J., Pouwels, P. H., Sára, M., Kotiranta, A., Lounatmaa, K., Kari, K., Kerosuo, E., Haapasalo, M., Egelseer, E. M., Schocher, I., Sleytr, U. B., Morelli, L., Callegari, M. L., Nomellini, J. F., Bingle, W. H., *et al.* (1997) Functions of S-layers. *FEMS Microbiol. Rev.* **20,** 99–149 CrossRef Medline
14. Rachel, R., Pum, D., Šmarda, J., Šmajs, D., Komrska, J., Krzyzánek, V., Rieger, G., and Stetter, K. O. (1997) Fine structure of S-layers. *FEMS Microbiol. Rev.* **20,** 13–23 CrossRef
15. Asif, M., Alvi, I. A., and Rehman, S. U. (2018) Insight into *Acinetobacter baumannii*: pathogenesis, global resistance, mechanisms of resistance, treatment options, and alternative modalities. *Infect. Drug Resist.* **11,** 1249–1260 CrossRef Medline
16. Hall, S. R., Shenton, W., Engelhardt, H., and Mann, S. (2001) Site-specific organization of gold nanoparticles by biomolecular templating. *Chemphyschem* **2,** 184–186 CrossRef Medline
17. Mark, S. S., Bergkvist, M., Yang, X., Teixeira, L. M., Bhatnagar, P., Angert, E. R., and Batt, C. A. (2006) Bionanofabrication of metallic and semiconductor nanoparticle arrays using S-layer protein lattices with different lateral spacings and geometries. *Langmuir* **22,** 3763–3774 CrossRef Medline
18. Fagan, R. P., and Fairweather, N. F. (2014) Biogenesis and functions of bacterial S-layers. *Nat. Rev. Microbiol.* **12,** 211–222 CrossRef Medline
19. Baranova, E., Fronzes, R., Garcia-Pino, A., Van Gerven, N., Papapostolou, D., Péhau-Arnaudet, G., Pardon, E., Steyaert, J., Howorka, S., and Remaut, H. (2012) SbsB structure and lattice reconstruction unveil Ca^{2+} triggered S-layer assembly. *Nature* **487,** 119–122 CrossRef Medline
20. Bharat, T. A. M., Kureisaite-Ciziene, D., Hardy, G. G., Yu, E. W., Devant, J. M., Hagen, W. J. H., Brun, Y. V., Briggs, J. A. G., and Löwe, J. (2017) Structure of the hexagonal surface layer on *Caulobacter crescentus* cells. *Nat. Microbiol.* **2,** 17059 CrossRef Medline
21. Baumeister, W., Karrenberg, F., Rachel, R., Engel, A., ten Heggeler, B., and Saxton, W. O. (1982) The major cell envelope protein of *Micrococcus radiodurans* (R1). Structural and chemical characterization. *Eur. J. Biochem.* **125,** 535–544 CrossRef Medline
22. Daly, M. J., Ouyang, L., Fuchs, P., and Minton, K. W. (1994) *In vivo* damage and recA-dependent repair of plasmid and chromosomal DNA in the radiation-resistant bacterium *Deinococcus radiodurans*. *J. Bacteriol.* **176,** 3508–3517 CrossRef Medline
23. White, O., Eisen, J. A., Heidelberg, J. F., Hickey, E. K., Peterson, J. D., Dodson, R. J., Haft, D. H., Gwinn, M. L., Nelson, W. C., Richardson, D. L., Moffat, K. S., Qin, H., Jiang, L., Pamphile, W., Crosby, M., *et al.* (1999) Genome sequence of the radioresistant bacterium *Deinococcus radiodurans* R1. *Science* **286,** 1571–1577 CrossRef Medline
24. Lin, J., Qi, R., Aston, C., Jing, J., Anantharaman, T. S., Mishra, B., White, O., Daly, M. J., Minton, K. W., Venter, J. C., and Schwartz, D. C. (1999) Whole-genome shotgun optical mapping of *Deinococcus radiodurans*. *Science* **285,** 1558–1562 CrossRef Medline
25. Makarova, K. S., Aravind, L., Wolf, Y. I., Tatusov, R. L., Minton, K. W., Koonin, E. V., and Daly, M. J. (2001) Genome of the extremely radiation-resistant bacterium *Deinococcus radiodurans* viewed from the perspective of comparative genomics. *Microbiol. Mol. Biol. Rev.* **65,** 44–79 CrossRef Medline
26. Levin-Zaidman, S., Englander, J., Shimoni, E., Sharma, A. K., Minton, K. W., and Minsky, A. (2003) Ringlike structure of the *Deinococcus radiodurans* genome: a key to radioresistance? *Science* **299,** 254–256 CrossRef Medline
27. Liu, Y., Zhou, J., Omelchenko, M. V., Beliaev, A. S., Venkateswaran, A., Stair, J., Wu, L., Thompson, D. K., Xu, D., Rogozin, I. B., Gaidamakova, E. K., Zhai, M., Makarova, K. S., Koonin, E. V., and Daly, M. J. (2003) Transcriptome dynamics of *Deinococcus radiodurans* recovering from ionizing radiation. *Proc. Natl. Acad. Sci. U.S.A.* **100,** 4191–4196 CrossRef Medline
28. Baumeister, W., Barth, M., Hegerl, R., Guckenberger, R., Hahn, M., and Saxton, W. O. (1986) Three-dimensional structure of the regular surface layer (HPI layer) of *Deinococcus radiodurans*. *J. Mol. Biol.* **187,** 241–250 CrossRef Medline
29. Rachel, R., Jakubowski, U., Tietz, H., Hegerl, R., and Baumeister, W. (1986) Projected structure of the surface protein of *Deinococcus radiodurans* determined to 8Å resolution by cryomicroscopy. *Ultramicroscopy* **20,** 305–316 CrossRef
30. Müller, D. J., Schoenenberger, C. A., Schabert, F., and Engel, A. (1997) Structural changes in native membrane proteins monitored at subnanometer resolution with the atomic force microscope: a review. *J. Struct. Biol.* **119,** 149–157 CrossRef Medline
31. Lister, T. E., and Pinhero, P. J. (2001) *In vivo* atomic force microscopy of surface proteins on *Deinococcus radiodurans*. *Langmuir* **17,** 2624–2628 CrossRef
32. Müller, D. J., Baumeister, W., and Engel, A. (1996) Conformational change of the hexagonally packed intermediate layer of *Deinococcus radiodurans* monitored by atomic force microscopy. *J. Bacteriol.* **178,** 3025–3030 CrossRef Medline
33. Farci, D., Bowler, M. W., Kirkpatrick, J., McSweeney, S., Tramontano, E., and Piano, D. (2014) New features of the cell wall of the radioresistant bacterium *Deinococcus radiodurans*. *Biochim. Biophys. Acta* **1838,** 1978–1984 CrossRef Medline
34. Peters, J., and Baumeister, W. (1986) Molecular cloning, expression, and characterization of the gene for the surface (Hpi)-layer protein of *Deinococcus radiodurans* in *Escherichia coli*. *J. Bacteriol.* **167,** 1048–1054 CrossRef Medline
35. Rothfuss, H., Lara, J. C., Schmid, A. K., and Lidstrom, M. E. (2006) Involvement of the S-layer proteins Hpi and SlpA in the maintenance of cell envelope integrity in *Deinococcus radiodurans* R1. *Microbiology* **152,** 2779–2787 CrossRef Medline
36. Farci, D., Bowler, M. W., Esposito, F., McSweeney, S., Tramontano, E., and Piano, D. (2015) Purification and characterization of DR_2577 (SlpA), a major S-layer protein from *Deinococcus radiodurans*. *Front. Microbiol.* **6,** 414 CrossRef Medline
37. Farci, D., Guadalupi, G., Bierła, K., Lobinski, R., and Piano, D. (2019) The role of iron and copper on the oligomerization dynamics of DR_2577, the

main S-layer protein of *Deinococcus radiodurans*. *Front. Microbiol.* **10,** 1450 CrossRef Medline
38. Sára, M., and Sleytr, U. B. (2000) S-layer proteins. *J. Bacteriol.* **182,** 859–868 CrossRef Medline
39. Dworkin, J., Tummuru, M. K., and Blaser, M. J. (1995) Segmental conservation of sapA sequences in type B *Campylobacter fetus* cells. *J. Biol. Chem.* **270,** 15093–15101 CrossRef Medline
40. Dworkin, J., Shedd, O. L., and Blaser, M. J. (1997) Nested DNA inversion of *Campylobacter fetus* S-layer genes is recA-dependent. *J. Bacteriol.* **179,** 7523–7529 CrossRef Medline
41. Farci, D., Esposito, F., El Alaoui, S., and Piano, D. (2017) S-layer proteins as a source of carotenoids: isolation of the protein cofactor deinoxanthin from its S-layer protein DR_2577. *Food Res. Int.* **99,** 868–876 CrossRef Medline
42. Vollan, H., Tannæs, T., Vriend, G., and Bukholm, G. (2016) *In silico* structure and sequence analysis of bacterial porins and specific diffusion channels for hydrophilic molecules: conservation, multimericity, and multifunctionality. *Int. J. Mol. Sci.* **17,** 599 CrossRef
43. Thornley, M. J., Glauert, A. M., and Sleytr, U. B. (1973) Isolation of outer membranes with an ordered array of subunits from *Acinetobacter*. *J. Bacteriol.* **115,** 1294–1308 Medline
44. Madhurantakam, C., Howorka, S., and Remaut, H. (2014) *S-layer Structure in Bacteria and Archaea* (Barton, L. L., Bazylinski, D., and Xu, H., eds), pp. 11–37, Springer, New York, NY
45. Sleytr, U. B., Schuster, B., Egelseer, E. M., and Pum, D. (2014) S-layers: principles and applications. *FEMS Microbiol. Rev.* **38,** 823–864 CrossRef Medline
46. Modi, N., Ganguly, S., Bárcena-Uribarri, I., Benz, R., van den Berg, B., and Kleinekathöfer, U. (2015) Structure, dynamics, and substrate specificity of the OprO porin from *Pseudomonas aeruginosa*. *Biophys. J.* **109,** 1429–1438 CrossRef Medline
47. Hille, B. (2007) *Ion Channels of Excitable Membranes*. Sunderland, MA
48. Kota, S., and Misra, H. S. (2008) Identification of a DNA processing complex from *Deinococcus radiodurans*. *Biochem. Cell Biol.* **86,** 448–458 CrossRef Medline
49. Hvidsten, T. R., Laegreid, A., Kryshtafovych, A., Andersson, G., Fidelis, K., and Komorowski, J. (2009) A comprehensive analysis of the structure–function relationship in proteins based on local structure similarity. *PLoS ONE.* **4,** e6266 CrossRef Medline
50. Benz, R., and Orlik, F. (2004) *Bacterial and Eukaryotic Porins: Structure, Function, Mechanism* (Roland Benz., ed) Wiley Interscience, New York
51. Forte, M., Adelsberger-Mangan, D., and Colombini, M. (1987) Purification and characterization of the voltage-dependent anion channel from the outer mitochondrial membrane of yeast. *J. Membr. Biol.* **99,** 65–72 CrossRef Medline
52. Ghai, I., Pira, A., Scorciapino, M. A., Bodrenko, I., Benier, L., Ceccarelli, M., Winterhalter, M., and Wagner, R. (2017) General method to determine the flux of charged molecules through nanopores applied to β-lactamase inhibitors and OmpF. *J. Phys. Chem. Lett.* **8,** 1295–1301 CrossRef Medline
53. Sotiropoulou, S., Mark, S. S., Angert, E. R., and Batt, C. A. (2007) Nanoporous S-layer protein lattices. A biological ion gate with calcium selectivity. *J. Phys. Chem. C* **111,** 13232–13237 CrossRef
54. Schwarzenlander, C., Haase, W., and Averhoff, B. (2009) The role of single subunits of the DNA transport machinery of *Thermus thermophilus HB27* in DNA binding and transport. *Environ. Microbiol.* **11,** 801–808 CrossRef Medline
55. Sutcliffe, I. C. (2010) A phylum level perspective on bacterial cell envelope architecture. *Trends Microbiol.* **18,** 464–470 CrossRef Medline
56. Arbing, M. A., Chan, S., Shin, A., Phan, T., Ahn, C. J., Rohlin, L., and Gunsalus, R. P. (2012) Structure of the surface layer of the methanogenic archaean *Methanosarcina acetivorans*. *Proc. Natl. Acad. Sci. U.S.A.* **109,** 11812–11817 CrossRef Medline
57. Etienne-Toumelin, I., Sirard, J. C., Duflot, E., Mock, M., and Fouet, A. (1995) Characterization of the *Bacillus anthracis* S-layer: cloning and sequencing of the structural gene. *J. Bacteriol.* **177,** 614–620 CrossRef Medline
58. Kern, J., Wilton, R., Zhang, R., Binkowski, T. A., Joachimiak, A., and Schneewind, O. (2011) Structure of surface layer homology (SLH) domains from *Bacillus anthracis* surface array protein. *J. Biol. Chem.* **286,** 26042–26049 CrossRef Medline
59. Eschweiler, B., Gerstenecker, B., Moriki, T., Bohrmann, B., and Kist, M. (1994) in *Basic and Clinical Aspects of Helicobacter pylori Infection* (Gasbarrini, G., and Pretolani, S., eds) Springer, Berlin, Heidelberg, Germany
60. Diatlov, I. A., and Antonova, O. A. (1999) The detection and characteristics of the *Yersinia pestis* antigen exhibiting the properties of S-layer proteins. *Zh Mikrobiol. Epidemiol. Immunobiol.* **4,** 90–91 Medline
61. Pei, Z., and Blaser, M. J. (1990) Pathogenesis of *Campylobacter fetus* infections. Role of surface array proteins in virulence in a mouse model. *J. Clin. Invest.* **85,** 1036–1043 CrossRef Medline
62. McConnell, M. J., Actis, L., and Pachón, J. (2013) *Acinetobacter baumannii*: human infections, factors contributing to pathogenesis and animal models. *FEMS Microbiol. Rev.* **37,** 130–155 CrossRef Medline
63. Murray, R. G. E. (1992) in *The Prokaryotes* (Balows, H. G., Dworkin, H., Harder, W., and Schleifer, K. H., eds) pp. 3732–3744, Springer, New York
64. Apweiler, R., Bairoch, A., and Wu, C. H. (2004) Protein sequence databases. *Curr. Opin. Chem. Biol.* **8,** 76–80 CrossRef Medline
65. UniProt Consortium. (2019) UniProt: a worldwide hub of protein knowledge. *Nucleic Acids Res.* **47,** D506–D515 CrossRef Medline
66. Söding, J. (2005) Protein homology detection by HMM-HMM comparison. *Bioinformatics* **21,** 951–960 CrossRef Medline
67. Hildebrand, A., Remmert, M., Biegert, A., and Söding, J. (2009) Fast and accurate automatic structure prediction with Hhpred. *Proteins* **77,** Suppl. 9, 128–132 CrossRef
68. Meier, A., and Söding, J. (2015) Automatic prediction of protein 3D structures by probabilistic multi-template homology modeling. *PLoS Comput. Biol.* **11,** e1004343 CrossRef Medline
69. Sievers, F., Wilm, A., Dineen, D., Gibson, T. J., Karplus, K., Li, W., Lopez, R., McWilliam, H., Remmert, M., Söding, J., Thompson, J. D., and Higgins, D. G. (2011) Fast, scalable generation of high-quality protein multiple sequence alignments using Clustal Omega. *Mol. Syst. Biol.* **7,** 539 CrossRef Medline
70. Källberg, M., Wang, H., Wang, S., Peng, J., Wang, Z., Lu, H., and Xu, J. (2012) Template-based protein structure modeling using the RaptorX web server. *Nat. Protoc.* **7,** 1511–1522 CrossRef Medline
71. Pettersen, E. F., Goddard, T. D., Huang, C. C., Couch, G. S., Greenblatt, D. M., Meng, E. C., and Ferrin, T. E. (2004) UCSF Chimera: a visualization system for exploratory research and analysis. *J. Comput. Chem.* **25,** 1605–1612 CrossRef Medline
72. Farci, D., Farci, S. F., Esposito, F., Tramontano, E., Kirkpatrick, J., and Piano, D. (2018) On the S-layer of *Thermus thermophilus* and the assembling of its main protein SlpA. *Biochim. Biophys. Acta* **1860,** 1554–1562 CrossRef Medline
73. Farci, D., Kirkpatrick, J., and Piano, D. (2017) A new procedure for fast soft staining of BN-PAGEs on photosynthetic complexes. *Electrophoresis* **38,** 441–446 CrossRef Medline
74. Zhang, K. (2016) Gctf: real-time CTF determination and correction. *J. Struct. Biol.* **193,** 1–12 CrossRef Medline
75. Tang, G., Peng, L., Baldwin, P. R., Mann, D. S., Jiang, W., Rees, I., and Ludtke, S. J. (2007) EMAN2: an extensible image processing suite for electron microscopy. *J. Struct. Biol.* **157,** 38–46 CrossRef Medline
76. Scheres, S. H. (2012) RELION: implementation of a Bayesian approach to cryo-EM structure determination. *J. Struct. Biol.* **180,** 519–530 CrossRef Medline
77. Haniewicz, P., Abram, M., Nosek, L., Kirkpatrick, J., El-Mohsnawy, E., Olmos, J. D. J., Kouřil, R., and Kargul, J. M. (2018) Molecular mechanisms of photoadaptation of Photosystem I supercomplex from an evolutionary cyanobacterial/algal intermediate. *Plant Physiol.* **176,** 1433–1451 CrossRef Medline
78. Cox, J., and Mann, M. (2008) MaxQuant enables high peptide identification rates, individualized p.p.b.-range mass accuracies, and proteome-wide protein quantification. *Nat. Biotechnol.* **26,** 1367–1372 CrossRef Medline
79. Cox, J., Neuhauser, N., Michalski, A., Scheltema, R. A., Olsen, J. V., and Mann, M. (2011) Andromeda: a peptide search engine integrated into the

MaxQuant environment. *J. Proteome Res.* **10,** 1794–1805 CrossRef Medline

80. Elias, J. E., and Gygi, S. P. (2007) Target-decoy search strategy for increased confidence in large-scale protein identifications by mass spectrometry. *Nat. Methods* **4,** 207–214 CrossRef Medline
81. Montal, M., and Mueller, P. (1972) Formation of bimolecular membranes from lipid monolayers and a study of their electrical properties. *Proc. Natl. Acad. Sci. U.S.A.* **69,** 3561–3566 CrossRef Medline
82. Vizcaíno, J. A., Csordas, A., del-Toro, N., Dianes, J. A., Griss, J., Lavidas, I., Mayer, G., Perez-Riverol, Y., Reisinger, F., Ternent, T., Xu, Q. W., Wang, R., and Hermjakob, H. (2016) 2016 update of the PRIDE database and its related tools. *Nucleic Acids Res.* **44,** D447–D456 CrossRef Medline
83. Deutsch, E. W., Csordas, A., Sun, Z., Jarnuczak, A., Perez-Riverol, Y., Ternent, T., Campbell, D. S., Bernal-Llinares, M., Okuda, S., Kawano, S., Moritz, R. L., Carver, J. J., Wang, M., Ishihama, Y., Bandeira, N., Hermjakob, H., and Vizcaíno, J. A. (2017) The ProteomeXchange consortium in 2017: supporting the cultural change in proteomics public data deposition. *Nucleic Acids Res.* **45,** D1100–D1106 CrossRef Medline
84. Perez-Riverol, Y., Csordas, A., Bai, J., Bernal-Llinares, M., Hewapathirana, S., Kundu, D. J., Inuganti, A., Griss, J., Mayer, G., Eisenacher, M., Pérez, E., Uszkoreit, J., Pfeuffer, J., Sachsenberg, T., Yilmaz, Ş. (2018) The PRIDE database and related tools and resources in 2019: improving support for quantification data. *Nucleic Acids Res.* **47,** D442—D450 CrossRef Medline